Impact of Annealing Temperature on Electrical Properties of Sol-gel $Ba_{0.90}Gd_{0.10}TiO_3$ Thin Films

Ala'eddin A. SAIF [1 *], Yen Chin TEH [2], Prabakaran POOPALAN [3]

[1] *Physics Department, College of Science, University of Jeddah, Jeddah, Saudi Arabia*
[2] *Infineon Technologies (Kulim) Sdn Bhd. Kedah, Malaysia*
[3] *School of Microelectronic Engineering, Universiti Malaysia Perlis, Pauh Putra, 02600, Arau, Perlis, Malaysia*

crossref http://dx.doi.org/10.5755/j02.ms.32220

Received 02 September 2022; accepted 27 September 2022

$Ba_{0.90}Gd_{0.10}TiO_3$ (BGT) thin films have been fabricated in MFM configuration via sol-gel technique at the different annealing temperature. The dielectric parameters of the films are measured using Impedance Analyzer as a function of frequency. It is found that, at frequency 1 kHz, the measured value of ε increases from 57 to 264 as the annealing temperature increases from 600 °C to 900 °C, which is correlated to the improved crystallinity and grain size increment. The ferroelectric hysteresis of the films is analyzed using Sawyer-Tower circuit that shows an enhancement for the ferroelectric properties with annealing temperature, which is also confirmed using C-V characteristics. The leakage current of the films is evaluated via Semiconductor Parameter Analyzer (SPA), which shows that at a certain electric field, the leakage current density increases as the annealing temperature increases, that is attributed to the crystallinity and grain size improvement. The conduction mechanism of the films is deeply investigated through different models to find out that the space charge limited conduction (SCLC) mechanism is the controlling conduction process.
Keywords: annealing temperature, $Ba_{0.90}Gd_{0.10}TiO_3$, conduction mechanism, dielectric, ferroelectric.

1. INTRODUCTION

Barium Titanate ($BaTiO_3$) is one of the non-toxic ferroelectric material that is widely used in the electronic industry due to its high dielectric constant, and excellent ferroelectric and piezoelectric properties at and above room temperature [1, 2]. Many studies suggest that doping $BaTiO_3$ with rare-earth elements, such as La, Sm and Gd, substitutes at the Ba^{2+} sites due to their larger atomic size compared to Ba^{2+}, resulting in lattice distortion and A-site vacancies. Such structural variations result in the improvement of some of the electrical properties of the $BatiO_3$ [3]. Li et al. observed a shift in the XRD peaks for Gd-doped BTO (Gd:BTO) powders, suggested that Gd ions substituted the Ba^{2+} ions when the Gd_2O_3 content in the precursor was less than 0.25 mol %, and they replaced both Ba and Ti ions when the Gd_2O_3 content in the precursor was greater than 0.25 mol %, which improve the dielectric constant at Gd content higher than 0.25 mol % [4]. It is also reported by Li et al. that Gadolinium (Gd^{3+}) doped $BaTiO_3$ has the largest dielectric constant compared with other rare-earth dopants used in their study [5]. Kang et al. depicted that the maximum value of dielectric constant (ε_{max}) of the Gd^{+3} doped $BaZrO_3$ is significantly increased, and the Curie temperature (T_C) shifted towards lower temperature, with the increase of Gd^{3+} doping till a certain doping ratio [6]. Similar results are observed by Said et al. for Strontium barium niobate doped with gadolinium, as well as, a relatively increment for the remnant polarization is noticed as Gd^{+3} doping concentration is increased [7].

Dielectric, ferroelectric and leakage current properties for Gd^{+3} doped $BaTiO_3$ thin films depend on various factors such as doping concentration, annealing temperature, film thicknesses, and fabrication condition [8 – 11]. However, the annealing temperature is the most important due to its direct relation to the crystalline structure of a material, which in turn influences the electrical conduction mechanism [12, 13].

Due to the limited works reported regarding Gd^{3+} doped $BaTiO_3$ thin films, the composite system is still unclear. Therefore, the effect of annealing temperature on their dielectric, ferroelectric and leakage mechanism need to be explored. In this study, $Ba_{0.90}Gd_{0.10}TiO_3$ (BGT) thin films have been fabricated in MFM configuration using sol-gel method and annealed at different temperatures. The dielectric, ferroelectric and leakage current mechanisms of the films then are deeply investigated as a function of annealing temperature and correlated to the structural properties.

2. METHODOLOGY

BGT solution is prepared using barium acetate (99 %), gadolinium acetate (99.9 %) and titanium (IV) isopropoxide (99.9 %) as raw materials. Acetic acid and 2-methoxyethanol were used as solvent and stabilizer, respectively. The details of solution preparation can be found in previous work [14]. For substrate preperation, a precleaned P-type silicon wafer (100) is used, then a 300 nm SiO_2 layer is grown on the wafer to act as a passivation layer, followed by a thin layer of TiO_2 with a thickness of ~ 3 nm is sputtered to serve as an adhesive layer between Pt and SiO_2 layers, finally, Pt layer with a thickness of 100 nm is sputtered onto the TiO_2 and followed by annealing at

* Corresponding author. Tel.: +966-5-95120706.
E-mail address: *aasaif@uj.edu.sa* (A.A. Saif)

800 °C for 1 hour to improve the crystallinity and conductivity of the platinum film. The $Ba_{0.9}Gd_{0.1}TiO_3$ solution is deposited on $Pt/TiO_2/SiO_2/Si$ substrates using a spin coater, and baked at 200 °C to harden the film and vaporize organic compounds, and then annealed at different temperatures of 600 °C, 700 °C, 800 °C and 900 °C, for 1 h in the atmosphere. For thickness measurement, the films with the structure of $BGT/Pt/TiO_2/SiO_2/Si$ are partially etched using diluted HF to create a step profile. Then the film thickness is measured using a profilometer (Stylus Profilometry, Bruker) with a force of 5 mg. The average film thickness is found to be 485.25±28 nm for all films. To obtain metal-ferroelectric-metal (MFM) structure for electrical characterization, the films are fabricated with the structure of $Al/BGT/Pt/TiO_2/SiO_2/Si$. Where, circular dots of aluminium electrode, with an area of 11.3×10^{-3} cm^2 are deposited over the $BGT/Pt/TiO_2/SiO_2/Si$ structure using PVD through a shadow mask to act as contact electrode. Thus, the under eath Pt layer serves as the bottom electrode while the aluminium dots on top of the BGT films serve as the top electrode as shown in Fig. 1.

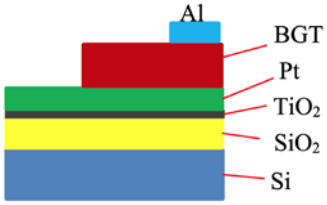

Fig. 1. Sample model structure

The perovskite structure for $Ba_{0.90}Gd_{0.10}TiO_3$ films on SiO_2/Si substrate was characterized by X-ray diffraction (XRD6000, Shimadzu) using Cu-ka radiation source (λ = 1.5406 Å), scan rate 2°/min and step size of 0.02° with an operating voltage of 40 kV and current of 30 mA. The grain size of BGT samples is measured using atomic force microscopy (AFM, SPA 400, SII Nanotechnology, Inc) in non-contact mode with a scan speed of 1 kHz. At least three locations on BGT films on SiO_2/Si substrate of an area of 1×1 μm^2 are scanned. Then the size of each grain is measured in diameter using Gwyddion software to ensure the accuracy of the measurement and then averaged. The dielectric properties of the films were characterized using the Impedance Analyzer (IM3570, Hioki) in the range from 100 Hz to 1 MHz at room temperature. The ferroelectric phenomenon of the films was analyzed using a homemade setup for the Sawyer-Tower circuit and Semiconductor Parameter Analyzer (4200A-SCS, Keithley). The leakage current for the present films was characterized in the range from 0 to 8 V using Semiconductor Parameter Analyzer.

3. RESULTS AND DISCUSSION

To confirm the presence of perovskite structure in $Ba_{0.90}Gd_{0.10}TiO_3$ thin films used in this work, XRD analysis has been employed and the patterns are plotted in the range between 20° and 60° as shown in Fig. 2. Comparable results for the current films with the previous work are obtained [14]. Where the sample annealed at 600°C shows an amorphous structure with no crystalline perovskite peak, suggesting poor crystallization of the film. The samples annealed at 700 °C, 800 °C and 900 °C confirmed the existence of perovskite phase structure through the formation of diffraction peaks with orientation (100), (110), (111), (200), (201) and (211). A single barium silicate peak, indicated by a blue square, is detected at 29° for the sample annealed at 900 °C only compared to the previous work that appeared at 800 °C also [14]. This indicates the improvement of the fabrication procedure of the films in this work. The lattice parameters of the current films annealed at different annealing temperatures are summarized in Table 1. From the table, a gradual increment of value is observed in the lattice constant of *a* and *c* with the increase in annealing temperature. This increment leads to expand the lattice volume from 63.49 to 63.62 $Å^3$. From the calculated lattice constants, it is also found that the ratio *c*/*a* is greater than 1 indicating that the tetragonal phase structure is obtained, which confirms the perovskite structure for the films.

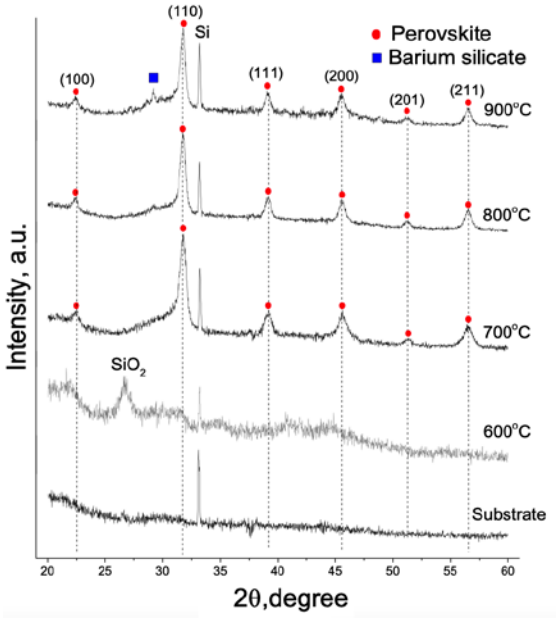

Fig. 2. XRD pattern of $Ba_{0.90}Gd_{0.10}TiO_3$ films annealed at different temperatures

Table 1. Lattice parameters of $Ba_{0.90}Gd_{0.10}TiO_3$ thin films at different annealing temperatures

Annealing temperature, °C	600	700	800	900
Lattice constant *a*, Å	ND	3.976±0.006	3.979±0.004	3.979±0.006
Lattice constant *c*, Å	ND	4.016±0.016	4.012±0.009	4.018±0.009
Tetragonality *c*/*a*	ND	1.01	1.01	1.01
Lattice volume *V*, $Å^3$	ND	63.497	63.530	63.616
*ND= no data				

Fig. 2 shows 1×1 μm^2 two-dimensional AFM images for $Ba_{0.90}Gd_{0.10}TiO_3$ films at various annealing temperatures. From the figure, dense and smooth surfaces with grains distributed evenly over the scan area are obtained for all the samples. However, no appearance of crystalline grain is found in the sample annealed at 600 °C (image not shown) due to insufficient annealing temperature. The measured average grain size for the samples annealed at 700 °C, 800 °C and 900 °C are 94.25 ± 1.19, 106.04 ± 1.21 and 154.20 ± 2.44, respectively. The increase of grain size with annealing

temperature is attributed to crystal growth with annealing temperature.

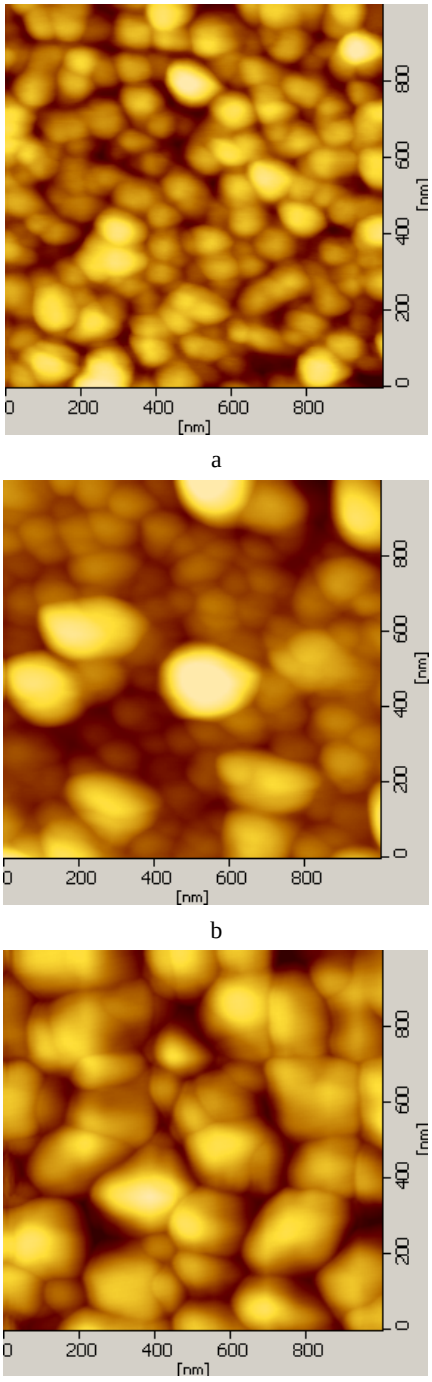

a

b

c

Fig. 3. Two-dimensional AFM images for $Ba_{0.90}Gd_{0.10}TiO_3$ films different annealing temperature: a – 700 °C; b – 800 °C; c – 900 °C

To investigate the influence of annealing temperature on the dielectric properties of the $Ba_{0.90}Gd_{0.10}TiO_3$ films, the real and imaginary parts of capacitance for the films with sample structure of MFM are measured as a function of frequency at room temperature. Then the real and imaginary parts of the dielectric constant are determined by the following equations, respectively:

$$\varepsilon' = \frac{Ct}{\varepsilon_0 A}; \quad (1)$$

$$\varepsilon'' = \frac{Gt}{\varepsilon_0 A\omega}, \quad (2)$$

where t is the film thickness; ω is the angular frequency; ε_o is the free space dielectric constant and A is the area of the top electrode.

The dielectric loss of the films, which represents the energy dissipation due to the lag of polarization behind the applied electric field caused by the impurities and imperfections with the lattice structure [15], is determined by the following equation:

$$tan\ \delta = \frac{\varepsilon''}{\varepsilon'}. \quad (3)$$

Fig. 4 a shows the variation of the real part of the dielectric constant as a function of frequency for $Ba_{0.90}Gd_{0.10}TiO_3$ thin films at the different annealing temperatures.

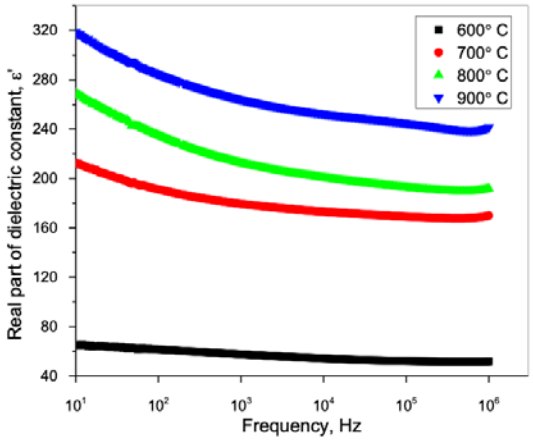

a

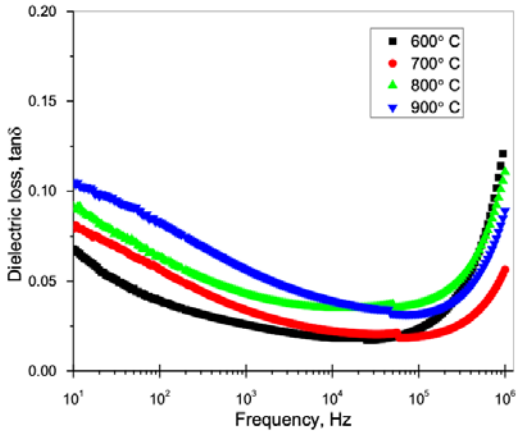

b

Fig. 4. a – dielectric constant; b – dielectric loss of $Ba_{0.90}Gd_{0.10}TiO_3$ films at the different annealing temperatures

The high value of the dielectric constant at low frequencies is due to space charge polarization, which is usually originated from the accumulation of charges at the grain boundaries and at the film/electrode interfaces. Then the dielectric constant decreases as the frequency increases for all the tested samples. This phenomenon can be explained by the nature of the dipole movement in the presence of the applied field. At low frequencies, the dipoles

orient according to the applied field at full strength of polarization. This explained the high value of ε′ at low frequency. However, these dipoles require a certain time to switch according to the oscillating field. Thus, as the frequency increases, leads to a shorter time for the switching, so the dipoles started to lag which slightly decreases ε′. At a very high frequency, the switch time for the applied field increases further, which means that the switching speed for the dipoles could not match the oscillating field. Thus, the ε′ remains almost constant and behaves as frequency independent at this range of frequencies.

It is also observed that the dielectric constant at a certain value of frequency increases with annealing temperature. For example; at 1 kHz, the dielectric constant increases from 57 to 264 for $Ba_{0.90}Gd_{0.10}TiO_3$ films as the annealing temperature increases from 600 °C to 900 °C. A similar increment of dielectric constant is also observed by Pečnik et al. [16] as they ascribed this increment to the improved crystallinity and the density of microstructure at the high annealing temperature. Quan et al., [17] explain that the combined effects of electric dipole polarization, the relaxed stress and strain, the improved crystallinity and large grain size are the main factors that caused the increase of dielectric constant with the increase of annealing temperature. Thus, the increase of the dielectric constant at the variation of annealing temperature in the current films is correlated to the improved crystallinity as discussed in XRD results, in addition, to the increase of grain size with annealing temperature.

The dependence of dielectric loss (tanδ) on frequency for $Ba_{0.90}Gd_{0.10}TiO_3$ films at different annealing temperatures is presented in Fig. 4 b. The figure shows that, at low frequencies < 10^3 Hz, the dielectric loss is slightly high and it dramatically decreases with frequency. The high value of tanδ at low frequencies is due to accumulated charge at the grain boundaries and film/electrode interfaces that harden the electrons transaction between the lattice sites, which in turn requires higher energy, thus, the loss would be higher [18]. At a higher frequency range, from 10^4 Hz to 10^5 Hz, tanδ becomes almost frequency independent and it is relatively low (< 0.5), which denotes the quality of the films. Furthermore, at higher frequencies, tanδ raises again to high values due to the miss switching speed of dipoles with the applied electric field at high frequencies. This sudden increment of tanδ at high frequencies indicates that a relaxation peak could be obtained [15].

The polarization of $Ba_{0.90}Gd_{0.10}TiO_3$ films with the structure of MFM is characterized through the Sawyer-Tower circuit by measuring the switchable polarization under an alternating electric field. When an electric field is applied, the dipoles re-oriented themselves according to the polarity of the field and induced the polarization strength. The polarization behavior under influence of annealing temperature is studied via polarization-electric field hysteresis loop analysis. Fig. 5 shows the hysteresis loop for $Ba_{0.90}Gd_{0.10}TiO_3$ films annealed at various annealing temperatures. It is found that samples annealed at 600 °C exhibit linear capacitor behavior. This indicated the absence of ferroelectricity due to the insufficient annealing temperature which is consistent with the XRD results.

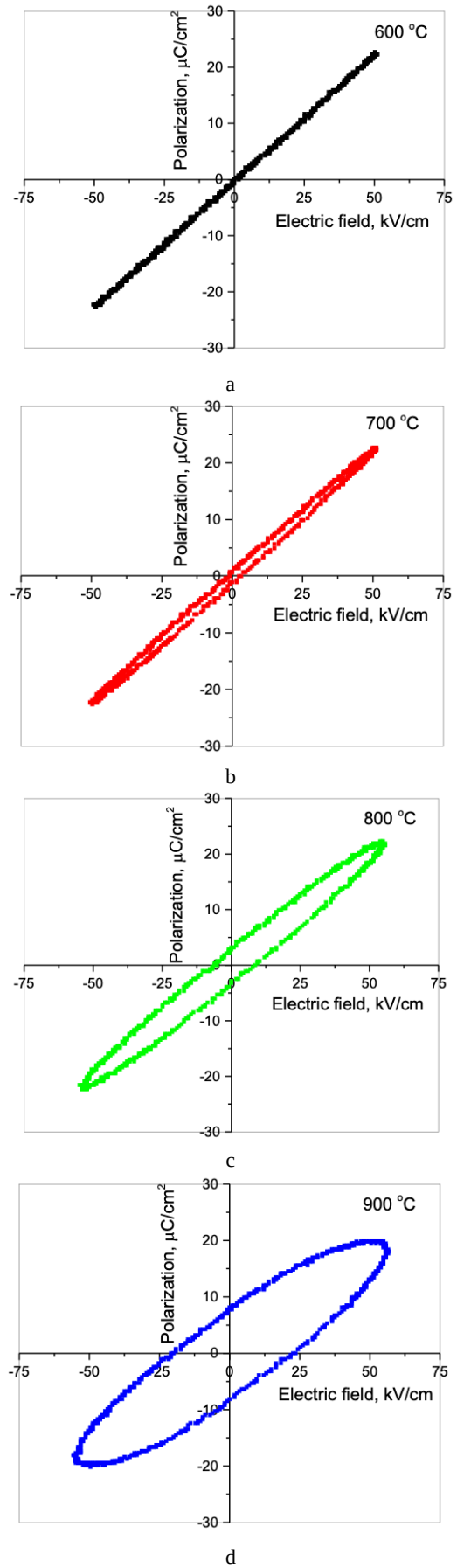

Fig. 5. Ferroelectric hysteresis loop of $Ba_{0.90}Gd_{0.10}TiO_3$ films annealed at different temperature: a – 600 °C; b – 700 °C; c – 800 °C; d – 900 °C

It can be also seen from the figure that the remnant polarization increased from 1 to 8.13 μC/cm^2 with the increased annealing temperature from 700 °C to 900 °C, indicating an improvement in the ferroelectric properties with annealing temperature. This enhancement in the ferroelectric properties of the current films is due to the improvement of the perovskite phase with annealing temperature, as discussed in XRD. Further, ferroelectric properties significantly depend on the grain size, where a larger grain size leads to reducing repulsive force between neighboring domain walls, thus, the ferroelectric films need lower activation energy for the reorientation of the domains [19]. As discussed earlier, the grain size of Gd-doped $BaTiO_3$ films increases with annealing temperature. This confirmed the improvement of the ferroelectric properties of the current films.

The ferroelectric properties of these films are also analyzed with the aid of capacitance-voltage (CV) characteristic to confirm their ferroelectricity. The CV for the films is characterized at 500 kHz in MFM configuration at room temperature. Where the applied DC voltage swept forward and reversed from - 6 to + 6 V with the sweeping rate of 0.1 V/s. Fig. 6 shows the capacitance-voltage graphs for $Ba_{0.90}Gd_{0.10}TiO_3$ annealed at distinct temperatures. It can be noted that all the films show a non-linear variation for capacitance with the applied voltage.

An anomalous C-V curve is observed at 600 °C which suggested the absence of ferroelectricity due to incomplete crystallinity. A similar C-V curve shape is also observed by Gao et al. for BMN films which are also due to the insufficient crystalline temperature at 600 °C [20]. It is also noted that the C-V curve is asymmetry around the voltage. Saif et al. [21] and Masruroh & Toda [22] reported that this shift could be originated from existing an accumulated charge at the film/electrode interface, and could be also due to the variation of work function for the bottom and top electrodes. Furthermore, two maxima peaks for the CV curve forming a butterfly shape is observed, that are attributed to polarization switching as a response to the sweeping voltage for both forward and reversed bias. The butterfly-like shape confirmed the presence of ferroelectric nature in the $Ba_{0.90}Gd_{0.10}TiO_3$ films at room temperature. The strength in the butterfly shape with the increase of annealing temperature is comparable with the obtained ferroelectric hysteresis loop. However, a distortion of the butterfly shape is observed for the sample annealed at 900 °C. This behavior could be due to the surface charge defects.

In many applications including microelectronic and optoelectronic, leakage current characteristics of thin films play a crucial part in examine the material parameters involved in the concentration of defects and quality of interfaces. Such applications required the leakage current to be as low as possible, wherein high leakage current could be led to the undesirable effects that limit performance. Therefore, it is essential to understand the conduction mechanism in the current films that control the required properties of the devices to be used for. The leakage current density of $Ba_{0.90}Gd_{0.10}TiO_3$ films is studied in a configuration of MFM structure with forward-biased on Al top electrode.

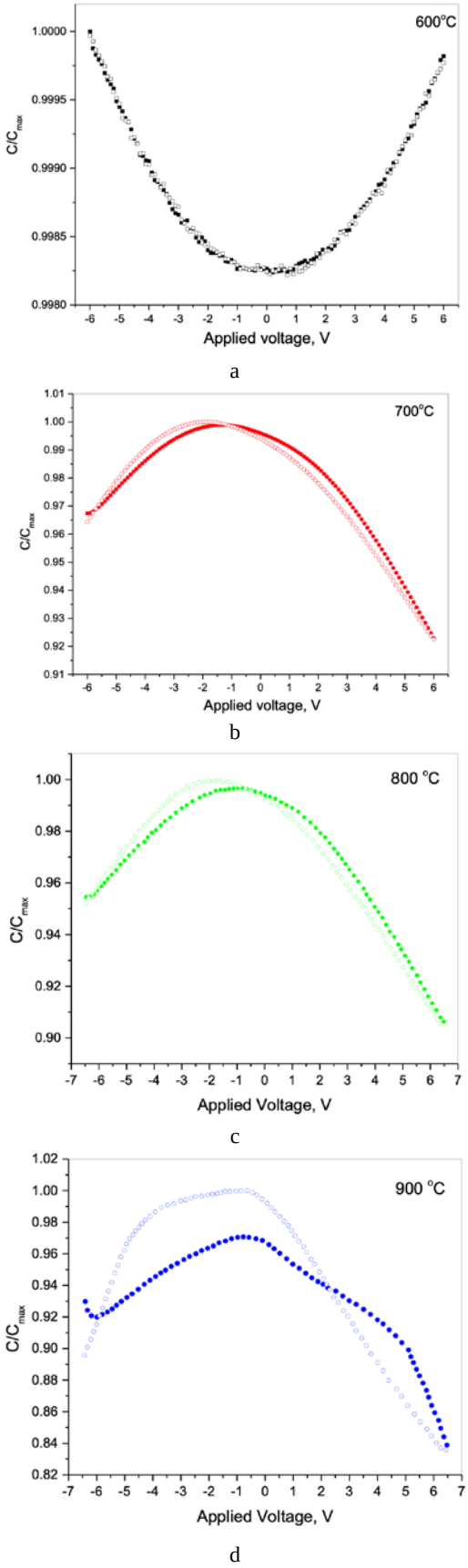

Fig. 6. C-V curve of $Ba_{0.90}Gd_{0.10}TiO_3$ films annealed: a – 600 °C; b – 700 °C; c – 800 °C; d – 900 °C

Fig. 7 illustrates the variation of leakage current density with the positive electric field for $Ba_{0.90}Gd_{0.10}TiO_3$ films

annealed at different temperatures. It is observed that at the fixed electric field of 100 kV/cm, the leakage current density increased from 2.16×10^{-5} to 3.39×10^{-4} A/cm^2 as the annealing temperature increased from 700 °C to 900 °C. Similar behavior is also observed by Sui et al. [23] in Fe doped NBT films and Gao et al. [20] in BMN thin films. They ascribed the increase of leakage current as a result of the formation of large grain at higher annealing temperature, which increases the conductivity between grains. Thus, the increase of the leakage current density in the $Ba_{0.90}Gd_{0.10}TiO_3$ films with the increase of annealing temperature is resulted from the improved crystallinity and larger grain size, which is consistent with the AFM results.

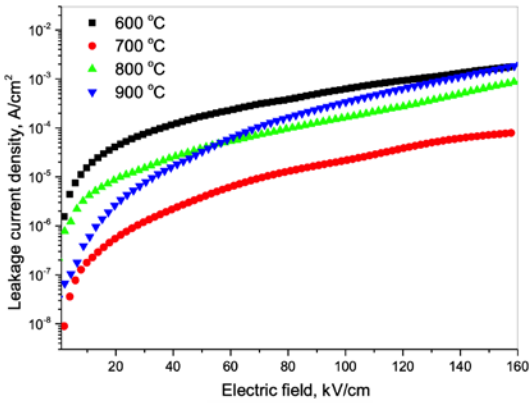

Fig. 7. Leakage current density as a function of the electric field of $Ba_{0.90}Gd_{0.10}TiO_3$ films at the different annealing temperatures

At a low electric field, < 20 kV/cm, the graph shows a linear variation for the current density with respect to the applied electric field indicating that the conduction mechanism in this range of electric fields is covered by Ohmic conduction. The current density due to the Ohmic conduction is formed due to the movement of mobile electrons in the conduction band and holes in the valence band as a response to the applied field. Ohmic current density usually is expressed as [24]:

$$J_{ohm} = qn_{\circ}\mu\frac{V}{d}, \tag{4}$$

where q is the electron charge; n_o is the concentration of the free charge carrier; μ is the carrier mobility; V is the applied voltage; d is the film thickness.

As the applied field increases further, > 20 kV/cm, more charges accumulate in the insulated regions from electrodes resulting in a further increase in leakage current, at this point, the space charge limited current conduction (SCLC) takes place. The current density at this stage is quadratic dependent on applied voltage according to Child's law which is given by [25]:

$$J = \frac{9\mu\varepsilon_{\circ}\varepsilon_r V^2}{8d^3}, \tag{5}$$

where ε_o is the permittivity of the free space and ε_r is the optical dielectric constant.

The SCLC mechanism within this range of the electric field is investigated via modified Langmuir-Child law. Where, according to Langmuir-Child law the conduction mechanism based on space charge limited (SCL) emission, the *J-E* characteristics for metal-ferroelectric-metal (MFM) capacitor system should follow the polynomial type of variation [26]. Fig. 8 shows the polynomial fitting of *J-E* plots for $Ba_{0.90}Gd_{0.10}TiO_3$ films at the different annealing temperatures. This indicates that the space charge mechanism is dominant for the tested films.

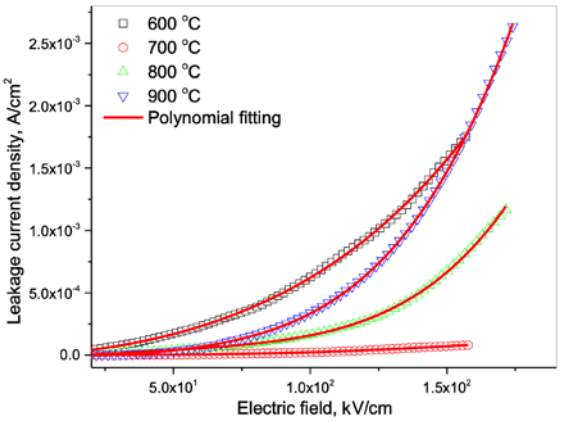

Fig. 8. Polynomial fitting of *J-E* plot for $Ba_{0.90}Gd_{0.10}TiO_3$ films at the different annealing temperature

The *J-E* plot, in Fig. 8, for all the tested films reveals that at a high applied field the leakage current almost increases exponentially with the applied field, indicating that other conduction mechanisms may present, where the Schottky emission (SE) and Poole–Frenkel (PF) emission have been considered [27]. The former occurs across the interface between a semiconductor/metal and an insulating film as a result of barrier lowering due to the applied field. The current density (J) in the Schottky emission can be quantified by the following equation [28]:

$$J = A^{*}T^{2}\exp\left[\frac{\beta_s E^{\frac{1}{2}} - \phi_s}{K_B T}\right], \tag{6}$$

where $\beta_s = (e^3/4\pi\varepsilon_o\varepsilon)^{1/2}$; e is the electron charge; ε_o is the dielectric constant of free space; ε is the dynamic dielectric constant; A^* is an effective Richardson constant; T is the absolute temperature, E the applied electric field, ϕ_s is the contact potential barrier; K_B is Boltzmann constant. The Poole-Frenkel emission is associated with the field enhanced thermal excitation of trapped electrons from the insulator into the conduction band. The current density according to PF emission is given by [28]:

$$J = J_o\exp\left[\frac{\beta_{PF} E^{\frac{1}{2}} - \phi_{PF}}{K_B T}\right]. \tag{7}$$

To investigate the possible contribution of Schottky emission and Poole-Frenkel emission at the higher electric field range, the *J-E* characteristic of $Ba_{0.90}Gd_{0.10}TiO_3$ films are plotted according to these models. Fig. 9 shows the *J-E* characteristic plotted according to Schottky emission plot of ln J versus $E^{1/2}$ for $Ba_{0.90}Gd_{0.10}TiO_3$ films at different annealing temperature. From the figure, a linear relationship

between ln J and $E^{1/2}$ is clearly seen which suggested that the Schottky emission may dominate over this range of electric field. However, in order to ensure the contribution of this mechanism, it is essential to determine the dynamic dielectric constant, ε_{SE}, from the slope of the linear fitting lines [30 – 39]. It is found that the extracted values of the dynamic dielectric constant from Schottky plot for the films tested at room temperature vary between 0.005 and 0.0129 demonstrating relatively low values. This could be indicated that the Schottky emission is not the dominant mechanism in $Ba_{0.90}Gd_{0.10}TiO_3$ films at room temperature [15].

Fig. 10 shows the variation of the *J-E* characteristic of $Ba_{0.90}Gd_{0.10}TiO_3$ films plotted according to Poole-Frenkel emission, ln (J/E) versus $E^{1/2}$. From the figure, a straight line fitting is observed for the current density but the estimated dynamic dielectric constant is also relatively low and varied from 0.031 to 0.165, which suggests that the Poole-Frenkel emission also is not the dominant conduction process in $Ba_{0.90}Gd_{0.10}TiO_3$ films at room temperature [15].

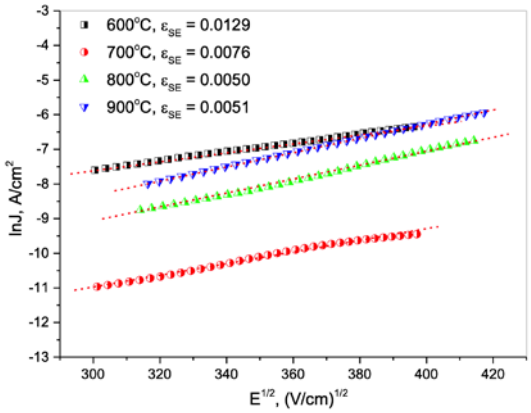

Fig. 9. Schottky emission plot of ln J vs $E^{1/2}$ for $Ba_{0.90}Gd_{0.10}TiO_3$ films at the different annealing temperatures

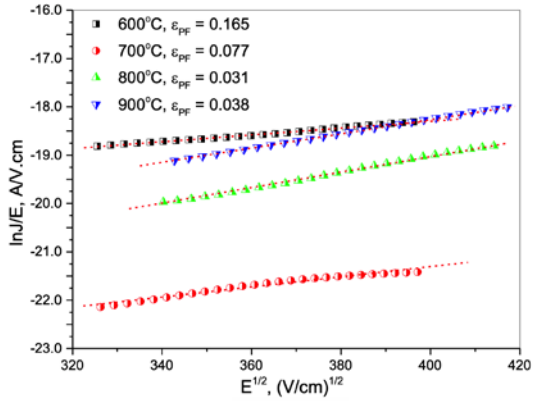

Fig. 10. Poole-Frenkel emission ln (J/E) vs $E^{1/2}$ for $Ba_{0.90}Gd_{0.10}TiO_3$ films at the different annealing temperatures

4. CONCLUSIONS

The dielectric, ferroelectric and leakage current properties of sol-gel $Ba_{0.90}Gd_{0.10}TiO_3$ thin films in MFM configuration have been investigated at the different annealing temperatures. The perovskite structure of $Ba_{0.90}Gd_{0.10}TiO_3$ films is checked with the aid of XRD, which reveals that the crystalline structure is improved as an annealing temperature increases. The dielectric constant ε of the films is plotted against frequency, and it is noticed that the measured values of ε at 1 kHz increase from 57 to 264 as the annealing temperature increases from 700 °C to 900 °C, which is correlated to the increment of grain size. The ferroelectric hysteresis loop and C-V curve of the films show an enhancement of the ferroelectric properties with annealing temperature. The estimated remnant polarization increases from 1 to 8.13 μC/cm^2 with the increase in annealing temperature from 700 °C to 900 °C. The leakage current measurement shows that the current density at the fixed electric field increases as the annealing temperature increases, which is correlated to the improvement of crystallinity and grain size. Additionally, it is found that space charge limited conduction (SCLC) is the dominant conduction mechanism within $Ba_{0.90}Gd_{0.10}TiO_3$ films.

REFERENCES

1. **Hernández Lara, J.P., Pérez Labra, M., Barrientos Hernández, F.R., Romero Serrano, J.A., Ávila Dávila, E.O., Thangarasu, P., Hernández Ramirez, A.** Structural Evolution and Electrical Properties of $BaTiO_3$ Doped with Gd^{3+} *Material Research* 20 (2) 2017: pp. 538 – 542. http://dx.doi.org/10.1590/1980-5373-mr-2016-0606
2. **Suchanicz, J., Konieczny, K., Świerczek, K., Lipiński, M., Karpierz, M., Sitko, D., Czternastek, H., Kluczewska, K.** Electrical Transport in Low-lead $(1–x)BaTiO_{3–x}PbMg_{1/3}Nb_{2/3}O_3$ Ceramics *Journal of Advanced Ceramics* 6 (3) 2017: pp. 207 – 219. https://doi.org/10.1007/s40145-017-0232-6
3. **Han-Sol, Y., Jae-Hyeon, Sh., Yong-Seon, K., Su-Yeon, K., So-Young, Sh., Kwon-Jin, P., Chun-Yeol, Y., Dae-Yong, J., Nam-Hee, Ch.** Structural and Chemical Features of Gd:$BaTiO_3$ Solid Solutions Prepared by Microwave-assisted Heat Treatment *Bulletin of Materials Science* 44 2021: pp. 241. https://doi.org/10.1007/s12034-021-02524-0
4. **Li, L., Wang, M., Guo, D., Fu, R., Meng, Q.** Effect of Gd Amphoteric Substitution on Structure and Dielectric Properties of BaTiO3-based Ceramics *Journal of Electroceramics* 30 2013: pp. 129 – 132. https://doi.org/10.1007/s10832-012-9773
5. **Li, Y., Hao, Y., Wang, X., Yao, X.** Studies of Dielectric Properties of Rare Earth (Y, Gd, Yb) Doped Barium Titanate Sintered in Pure Nitrogen *Ferroelectrics* 407 (1) 2010: pp. 134 – 139. https://doi.org/10.1080/00150193.2010.484757
6. **Kang, W., Zheng, Z., Li, Y.** Effect of Doping Gd_2O_3 on Dielectric and Piezoelectric Properties of $BaZr_{0.1}Ti_{0.9}O_3$ Ceramics by Sol–gel Method *Journal of Materials Science: Materials in Electronics* 30 2019: pp. 2743 – 2749. https://doi.org/10.1007/s10854-018-0550-7
7. **Said, M., Velayutham, T.S., Abd Majid, W.H.** Dielectric, Pyroelectric, Ferroelectric Properties Gadolinium Doped $Sr_{0.53}Ba_{0.47}Nb_2O_6$ Ceramic *Ceramic International* 43 (13) 2017: pp. 9783 – 9789. https://doi.org/10.1016/j.ceramint.2017.04.156
8. **Maneeshya, L.V., Lekshmy, S.S., Thomas, P.V., Joy, K.** Europium Incorporated Barium Titanate Thin Flms for Optical Applications *Journal of Materials Science: Materials in Electronics* 25 2014: pp. 2507 – 2515. http://dx.doi.org/10.1007/s10854-014-1903-5

9. **Dongyun, G., Yunbo, W., Jun, Y., Junxiong, G.** Effect of Annealing on Ferroelectric Properties of $Bi_{3.25}La_{0.75}Ti_3O_{12}$ Thin Films Prepared by the Sol-gel Method *Journal of Wuhan University of Technology (Materials Science)* 20 2005: pp. 20 – 21. https://doi.org/10.1007/BF02841273
10. **Gheidari, A.M., Soleimani, E.A., Mansorhoseini, M.** Structural Properties of Indium Tin Oxide Thin Flms Prepared for Application in Solar Cells *Materials Research Bulletin* 40 (8) 2005: pp. 1303 – 1307. http://dx.doi.org/10.1016/j.materresbull.2005.04.007
11. **Sankara, P.S., Munroe, P.R.** Influence of Fabrication Conditions on the Ferroelectric Polarization of Barium Titanate Thin Films *Journal of Asian Ceramics Society* 1 (2) 2013: pp. 149 – 154. https://doi.org/10.1016/j.jascer.2013.04.001
12. **Khanal, G.P., Kim, S., Fujii, I., Ueno, Sh., Moriyoshi, Ch., Kuroiwa, Y., Wada, S.** Effect of Thermal Annealing on Crystal Structures and Electrical Properties in $BaTiO_3$ Ceramics *Journal of Applied Physics* 124 (3) 2018: pp. 034102. https://doi.org/10.1063/1.5023814
13. **Caruntu, G., Rarig, R., Dumitru, I., O'Connor, C. J.** Annealing Effects on the Crystallite Size and Dielectric Properties of Ultrafine $Ba_{1-x}Sr_xTiO_3 (0 < x < 1)$ Powders Synthesized Through an Oxalate-Complex Precursor *Journal of Material Chemistry* 16 (8) 2006: pp. 752 – 758. https://doi.org/10.1039/B506578J
14. **Teh, Y.C., Saif, A.A.** Influence of Annealing Temperature on Structural and Optical Properties of Sol-gel Derived $Ba_{0.9}Gd_{0.1}TiO_3$ Thin Films for Optoelectronics *Journal of Alloys and Compounds* 703 2017: pp. 407 – 413. http://dx.doi.org/10.1016/j.jallcom.2017.01.312
15. **Saif, A.A., Teh, Y.C.** Correlation of Ba:Gd Ratio and Film Thickness to the Dielectric, Ferroelectric and Leakage Current Mechanism of Nanostructure $Ba_{1-x}Gd_xTiO_3$ Thin Films *Physica B* 612 2021: pp. 412824. https://doi.org/10.1016/j.physb.2021.412824
16. **Pečnik, T., Glinšek, S., Kmet, B., Malič, B.** Solution-Derived $Ba_{0.5}Sr_{0.5}TiO_3$ Thin Film Capacitors in Metal-Insulator-Metal Configuration *Informacije MIDEM* 46 (3) 2016: pp. 136 – 141.
17. **Quan, Z., Hu, H., Guo, S., Liu, W., Xu, S., Huang, H.** Effect of Annealing Temperature on Microstructure, Optical and Electrical Properties of Sputtered $Ba_{0.9}Sr_{0.1}TiO_3$ Thin Films *Applied Surface Science* 255 (22) 2009: pp. 9045 – 9053. https://doi.org/10.1016/j.apsusc.2009.06.096
18. **Srinivasamurthy, K.M., Manjunatha, K., Sitalo, E.I., Kubrin, S.P., Sathish, I.C., Matteppanavar, S.** Effect of Ce^{3+} Substitution on the Structural, Morphological, Dielectric, and Impedance Spectroscopic Studies of Co–Ni Ferrites for Automotive Applications *Indian Journal of Physic* 94 2020: pp. 593 – 604. https://doi.org/10.1007/s12648-019-01495-7
19. **Ngo-Duc, Q., Tran-Quoc, T., Vu-Ngoc, H., Minh-Duc, N.** Influence of Crystallization Temperature on Structural, Ferroelectric, and Ferromagnetic Properties of Lead-Free $Bi_{0.5}(Na_{0.8}K_{0.2})_{0.5}TiO_3$ Multiferroic Films *Advances in Materials Science and Engineering* 2019: pp. 8976385. https://doi.org/10.1155/2019/8976385
20. **Gao, L., Jiang, S., Li, R., Li, B., Li, Y.** Structure and Dielectric Properties of Sputtered Bismuth Magnesium Niobate Thin Films *Thin Solid Films* 520 (19) 2012: pp. 62956298. https://doi.org/10.1016/j.tsf.2012.06.035
21. **Saif, A.A., Jamal, Z.A.Z., Poopalan, P.** Effect of the Chemical Composition at the Memory Behavior of Al/BST/SiO_2/Si-gate-FET Structure *Applied Nanoscience* 1 2011: pp. 157 – 162. https://doi.org/10.1007/s13204-011-0024-1
22. **Masruroh, M.T.** Asymmetric Hysteresis Loops, Leakage Current and Capacitance Voltage Behaviors in Ferroelectric PZT Films Deposited on a Pt/Al_2O_3/SiO_2/Si Substrate by MOCVD Method with a Vapor-deposited Gold Top Electrode *International Journal of Applied Physics and Mathematics* 1 (2) 2011: pp. 144 – 148. https://doi.org/10.7763/IJAPM.2011.V1.28
23. **Sui, H., Yang, C., Zhao, M., Lin, W., Feng, C.** Effects of Annealing Temperature on the Microstructure, Electrical Properties of Fe-Doped $Na_{0.5}Bi_{0.5}TiO_3$ Thin Films *Journal of Alloys and Compounds* 586 2014: pp. 683 – 687. https://doi.org/10.1016/j.jallcom.2013.10.117
24. **Wu, X., Dong, Sh., Zhai, Y., Xu, M., Kan, Y.** Testing Field and Annealing Temperature Dependence of Leakage Current Properties in $Bi_{3.25}La_{0.75}Ti_3O_{12}$ Thin Films *Thin Solid Films* 519 (7) 2011: pp. 2376 – 2380. https://doi.org/10.1016/j.tsf.2010.11.021
25. **Liu, C.F., Tang, X.G., Wang, L.Q.** Resistive Switching Characteristics of HfO_2 Thin Films on Mica Substrates Prepared by Sol-Gel Process *Nanomaterials (Basel, Switzerland)* 9 (8) 2019: pp. E1124. https://doi.org/10.3390%2Fnano9081124
26. **Chen, M.J., Ning, X.K., Wang, S.F., Fu, G.S.** Enhanced Polarization and Dielectricity in $BaTiO_3$:NiO Nanocomposite Films Modulated by the Microstructure *RSC Advances* 7 2017: pp. 38231 – 38242. https://doi.org/10.1039/C7RA06627A
27. **Fan, S., Wang, C., Xie, X., Guo, X.** Improvement of Leakage and Ferroelectric Properties of Mn-doped $BiFeO_3$ Thin Films *Journal of Ceramic Processing Research* 18 (4) 2017: pp. 301 – 304. https://doi.org/10.1063/1.3098408
28. **Fu-Chien, Ch.** A Review on Conduction Mechanisms in Dielectric Films *Advances in Materials Science and Engineering* 2014: pp. 578168. https://doi.org/10.1155/2014/578168
29. **Yu, C.C., Kao, M.C., Chen, H.Z., Young, S.L., Lin, C.H.** Electrical Properties and Leakage Current Mechanisms of $Bi_{3.2}Gd_{0.8}Ti_3O_{12}$ Thin Films Prepared by a Sol-gel Method *Journal of* Superconductivity *and Novel Magnetism* 23 (6) 2010: pp. 929 – 932. https://doi.org/10.1007/s10948-009-0612-4
30. **Kim, H.K., Lee, S.H., In Kim, S., Woo Lee, C., Rag Yoon, J., Lee, S.G., Lee, Y.H.** Dielectric Strength of Voidless $BaTiO_3$ Films with Nano-scale Grains Fabricated by Aerosol Deposition *Journal of Applied Physics* 115 (1) 2014: pp. 1 – 6. https://doi.org/10.1063/1.4851675
31. **Qi, H., Wang, H., Xu, X., Tang, Y., Xiao, P., Xiao, M.** Microstructure and Electrical Properties of Ferroelectric $Bi_{3.15}Nd_{0.85}Ti_3O_{12}$/$BiFeO_3$/$Bi_{3.15}Nd_{0.85}Ti_3O_{12}$ Trilayered Thin Films on Pt/Ti/SiO_2/Si *Journal of Materials Science: Materials in Electronics* 28 2017: pp. 13757 – 13762. https://doi.org/10.1007/s10854-017-7220-z